INTERNATIONAL JOURNAL OF OPTIMIZATION IN CIVIL ENGINEERING
Int. J. Optim. Civil Eng., 2025; 15(1):15-37

GEOMETRIC AND SIZE OPTIMIZATION OF STRUCTURES UNDER NATURAL FREQUENCY CONSTRAINTS USING IMPROVED MATERIAL GENERATION ALGORITHM

V. Goodarzimehr[1*, †], N. Fanaie[2], S. Talatahari[3,4]
[1] *Faculty of Civil Engineering and Architecture, Shahid Chamran University of Ahvaz, Ahvaz, Iran*
[2] *Department of Civil Engineering, K. N. Toosi University of Technology, Tehran, Iran*
[3] *School of Computing, Macquarie University, Sydney, Australia*
[4] *Department of Computer Science, Khazar University, Baku, Azerbaijan*

ABSTRACT

In this study, the Improved Material Generation Algorithm (IMGA) is proposed to optimize the shape and size of structures. The original Material Generation Algorithm (MGA) introduced an optimization model inspired by the high-level and fundamental characteristics of material chemistry, particularly the configuration of compounds and chemical reactions for generating new materials. MGA uses a Gaussian normal distribution to produce new combinations. To enhance MGA for adapting truss structures, a new technique called Random Chaotic (RC) is proposed. RC increases the speed of convergence and helps escape local optima. To validate the proposed method, several truss structures, including a 37-bar truss bridge, a 52-bar dome, a 72-bar truss, a 120-bar dome, and a 200-bar planar structure, are optimized under natural frequency constraints. Optimizing the shape and size of structures under natural frequency constraints is a significant challenge due to its complexity. Choosing the frequency as a constraint prevents resonance in the structure, which can lead to large deformations and structural failure. Reducing the vibration amplitude of the structure decreases tension and deflection. Consequently, the weight of the structure can be minimized while keeping the frequencies within the permissible range. To demonstrate the superiority of IMGA, its results are compared with those of other state-of-the-art metaheuristic methods. The results show that IMGA significantly improves both exploitation and exploration.

Keywords: Dynamic Constraint, Metaheuristic Algorithms, Truss Optimization, Soft

[*]Corresponding author: Faculty of Civil Engineering and Architecture, Shahid Chamran University of Ahvaz, Ahvaz, Iran
[†]E-mail address: v.goodarzimehr@scu.ac.ir (V. Goodarzimehr)

Computing, Natural Frequency Constraints.

Received: 14 December 2024; Accepted: 20 January 2025

1. INTRODUCTION

Due to the physical nature of structural problems, the constraints of these problems are classified as behavior constraints and lateral constraints. These constraints limit the search space and add complexity to the convergence of the response vector towards the global optimum. Behavior constraints include stress, displacement, and frequency. Typically, the cross-sectional area of the members is also used as a lateral constraint, which defines the domain of the feasible search space. Therefore, the weight of truss structures can be minimized without compromising their stability. The following sections describe the optimization of structures using metaheuristic algorithms.

Metaheuristic algorithms are popular tools for optimizing constrained problems due to their simplicity, flexibility, and lack of need for derivative information. These algorithms can efficiently find the optimal solution through an iterative process. Some of the most important methods are highlighted: Pulluri et al. (2016) [1] presented a new Colliding Bodies Optimization (CBO) based on energy laws for optimizing engineering and numerical problems. Mirjalili et al. (2016) [2] proposed a Multi-Verse Optimizer (MVO), inspired by cosmological concepts of white holes, black holes, and wormholes, to find optimal solutions for engineering and numerical problems. Abualigah et al. (2021) [3] introduced the Arithmetic Optimization Algorithm (AOA), which uses arithmetic operators to solve both constrained and unconstrained problems. Faramarzi et al. (2019) [4] developed the Equilibrium Optimizer (EO), inspired by control volume mass balance models, for solving numerical problems. Goodarzimehr et al. (2022) [5] introduced the Special Relativity Search (SRS) algorithm for optimizing a wide range of feasible spaces. Bayzidi et al. (2021) [6] developed Social Network Search (SNS) for solving optimization problems with both continuous and discrete variables. Yang et al. (2021) [7] developed Hunger Games Search (HGS) for optimizing both constrained and unconstrained problems. Wang (2018) [8] introduced the Moth Search (MS) algorithm for optimizing numerical and engineering problems. Heidari et al. (2019) [9] proposed the Harris Hawks Optimizer (HHO), inspired by Harris' hawks behavior, for solving real-world and numerical problems. Heidari et al. (2019) [9] proposed the Harris Hawks Optimizer (HHO), inspired by Harris' hawks behavior, for solving real-world and numerical problems. Li et al. (2020) [11] introduced the Slime Mould Algorithm (SMA) for optimal design in engineering problems. Chen et al. (2021) [12] utilized Particle Swarm Optimization (PSO) for designing non-trivial flat-foldable origami tessellations. Abualigah et al. (2022) [13] proposed the Reptile Search Algorithm (RSA), mimicking crocodile hunting behavior, for optimal design in numerical and engineering problems. Tu et al. (2021) [14] developed the Colony Predation Algorithm (CPA), inspired by animal corporate behavior. Azizi et al. (2022) [15] introduced a new metaheuristic algorithm inspired by the behavior of three bird species: whistling kites, black kites, and brown falcons, for optimizing numerical problems. Talatahari et al. (2021a) [16]

proposed the Crystal Structure Algorithm (CryStAl) based on crystal formation. All these methods are single-objective and population-based, widely used to solve various problems.

Structural optimization under behavior constraints of stress and displacement ensures that the stress on any member and the displacement at any node do not exceed allowed values. This maintains the structure's stability and resistance against forces while minimizing weight. Key methods for optimizing truss structures under these constraints include: Javidi et al. (2019) [17] introduced the Enhanced Crow Search Algorithm (ECSA) for truss optimization under stress and displacement constraints. Jafari et al. (2019) [18] developed a hybrid method for optimizing truss structures with these constraints. Cao et al. (2017) [19] enhanced Particle Swarm Optimization (EPSO) for structural design. Kaveh and Zakian (2018) [20] improved the Grey Wolf Optimizer for space structure design. Degertekin et al. (2017) [21] adapted Heat Transfer Search (HTS) for truss weight minimization. Kaveh et al. (2020) [22] used Advanced Charged System Search (ACSS) for optimizing large structures. Lee and Geem (2004) [23] introduced Harmony Search for structural optimization. Degertekin et al. (2020) [24] used School-Based Optimization (SBO) to optimize structures under earthquake forces. Goodarzimehr et al. (2022) [25] presented a hybrid metaheuristic for optimizing space and planar trusses. Goodarzimehr et al. (2025) [26] used a hybrid method for frequency optimization. Topal et al. (2022) [27] introduced a hybrid method for optimizing laminated structures. Talatahari et al. (2021b) [28] hybridized Symbiotic Organism Search and Harmony Search for optimal design with discrete variables. Goodarzimehr et al. (2024) [29] used SRS for optimization of composite plates with continuous variables. Most metaheuristic methods have successfully found optimal solutions for structural optimization problems.

Optimization under frequency constraints, due to non-linearity, non-convexity, and vibration control, remains complex and costly. Thus, developing an efficient, accurate method with low computational cost is still an open issue. Notable contributions in this area include: Wang et al. (2004) [30] introduced the Optimality Criterion (OC) for optimizing structures under frequency, displacement, and stress constraints. Wei et al. (2005) [31] increased population diversity to address non-linear, frequency-sensitive optimization. Gomes (2011) [32] modified Particle Swarm Optimization (PSO) for truss optimization with natural frequency constraints. Miguel (2012) [33] adapted Harmony Search (HS) and Firefly Algorithm (FA) for frequency-constrained structural optimization. Kaveh and Mahdavi (2014) [34] developed Colliding Bodies Optimization (CBO) for frequency constraint problems. Kaveh and Zolghadr (2014) [35] introduced Democratic PSO (DPSO) to improve PSO for frequency-constrained structural optimization. Farshchin et al. (2016) [36] developed Multi-class Teaching-Learning Based Optimization (MCTLBO) for truss optimization with natural frequency constraints. Tejani et al. (2016) [37] improved Symbiotic Organisms Search (SOS) for frequency-constrained optimization. Lin et al. (1982) [38] used the Kuhn-Tucker method for frequency-constrained structural optimization. Kaveh and Zolghadr (2012) [39] complemented the CSS algorithm with BB-BC for faster convergence in frequency-constrained optimization. Khatibinia and Naseralavi (2014) [40] introduced the Multi-Gravitational Search Algorithm (OMGSA) for optimal design with frequency constraints. Kaveh and Mahdavi (2015) [41] modified the colliding bodies algorithm for two-dimensional optimization. Mortazavi (2021) [42] utilized an interactive

fuzzy search algorithm for dynamic constraint optimization. Goodarzimehr et al. (2022) [43] developed hybrid PSOGA for optimizing geometrically nonlinear space structures. Kaveh and Talatahari [44, 45] have developed a CSS based on new strategies for structural optimization, specifically for truss structures. Due to the complexity and presence of multiple local optima, efficient metaheuristic methods are still needed for these problems.

This study proposes the Improved Material Generation Algorithm (IMGA) for optimizing truss structures with natural frequency constraints. The Material Generation Algorithm (MGA) [46], a recent metaheuristic, is based on material combination for new composition creation. However, MGA's limitation to existing compounds causes local optima traps and slow convergence. The Random Chaotic (RC) technique is introduced to enhance diversity in new material production. Problems with multiple frequency constraints, including a 37-bar truss bridge, a 52-bar dome, a 72-bar structure, a 120-bar dome, and a 200-bar planar structure, are used to demonstrate IMGA's capabilities. Comparative results show that IMGA improves convergence speed and avoids local optima more effectively than other metaheuristic methods.

2. IMPROVED MATERIAL GENERATION ALGORITHM

The Material Generation Algorithm (MGA) is a single-objective, population-based metaheuristic inspired by the science of combining materials to create new ones with improved characteristics. In reality, different materials are combined to meet specific needs, resulting in new materials with enhanced properties and performance. While the fundamental structure of materials cannot be altered, they can be improved at atomic, nano, micro, or macro scales for engineering purposes. These improvements are guided by chemical reactions, making material chemistry a crucial field for producing materials with superior characteristics. By replacing or transferring electrons between atoms, new substances can be generated. The MGA utilizes this concept to develop a metaheuristic algorithm for optimizing single-objective problems through three phases: Chemical Compound, Chemical Reaction, and Chemical Stability.

Before detailing the three main phases of the MGA, it is important to explain the mathematical modeling of the proposed algorithm. Similar to other population-based methods, MGA begins the optimization process by generating an initial random population. As described by Eq. (1), MGA creates a population of different materials (Mat), each containing various decision variables (PTE_i^j). Like other metaheuristic methods, MGA uses specific operators and randomly selects a number of decision variables within the feasible space.

$$Mat = \begin{bmatrix} Mat_1 \\ Mat_2 \\ \vdots \\ Mat_i \\ \vdots \\ Mat_n \end{bmatrix} = \begin{bmatrix} PTE_1^1 & PTE_1^2 & \cdots & PTE_1^j & \cdots & PTE_1^d \\ PTE_2^1 & PTE_2^2 & \cdots & PTE_2^j & \cdots & PTE_d^d \\ \vdots & \vdots & \vdots & \vdots & \vdots & \vdots \\ PTE_i^1 & PTE_i^2 & \cdots & PTE_i^j & \cdots & PTE_i^d \\ \vdots & \vdots & \vdots & \vdots & \vdots & \vdots \\ PTE_n^1 & PTE_n^2 & \cdots & PTE_n^j & \cdots & PTE_n^d \end{bmatrix}, \quad \begin{cases} i = 1, 2, ..., n \\ j = 1, 2, ..., d \end{cases} \tag{1}$$

where n is the number of different material compounds generated randomly, d is the number of variables, which depends on the problem.

The initial vector of possible optimal answers PTE is calculated using Eq. (2). Like other metaheuristic methods, the MGA is randomly selecting the candidates between lower and upper bound for all different Mats.

$$PTE_i^j = PTE_{i,\min}^j + unif(0,1)(PTE_{i,\max}^j - PTE_{i,\min}^j), \qquad \begin{cases} i = 1,2,...,n \\ j = 1,2,...,d \end{cases} \tag{2}$$

where PTE_i^j indicates the initial value of the j[th] variable in the i[th] *Mat*; *unif(0,1)* is a random value selected in the range (0,1), $PTE_{i,max}^j$ and $PTE_{i,min}^j$, are the minimum and maximum allowable values for the j[th] variable of the i[th] optimum candidate, respectively.

Phase 1; Chemical Compound: In the proposed model for chemical composition, it is assumed that, similar to a magnetic field, energy absorption and ion interactions occur with one another. Depending on the stability of different elements, electrons tend to be shared or transferred between elements, forming covalent bonds. Eq. (3) is defined to model these covalent compounds. Probabilistic theory is used to model the loss or sharing of ions.

$$PTE_{new}^k = PTE_{r_1}^{r_2} \pm e^- , \quad k = 1,2,...,d \tag{3}$$

where PTE_{new}^k is a newly generated material, $PTE_{r_1}^{r_2}$ is a selected material with r_1 and r_2 uniformly distributed random integers in the range [1,n] and [1,d], respectively. e is the probabilistic value for modeling the process of losing, gaining or sharing electrons.

Phase 2; Chemical Reaction: A chemical reaction is a process where the structure of the constituent elements of raw materials changes, converting one or more chemicals into different chemicals. Unlike physical changes, where only the physical state of the substance changes without altering its elemental structure, chemical reactions alter the actual composition. In the proposed mathematical model for chemical reactions, an integer random number (l) is used to determine participation in the reaction, depending on the type of initial material (Mat). A new random number is chosen to locate the material, forming a linear combination of other solutions. The participation coefficient (p) is used to model the involvement of materials with different values. Eq. (4) describes the chemical reaction phase.

$$Mat_{new_2} = \frac{\sum_{m=1}^{l}(p_m . Mat_{mj})}{\sum_{m=1}^{l}(p_{mj})} , \quad j = 1,2,...,l \tag{4}$$

where Mat_{new_2} is a newly generated material, the p_m is a random integer with normal distributuion, Mat_{mj} is the i^{th} randomly selected material from initial *Mat* .

Phase 3; Chemical Stability: Material stability depends on system behavior, which is influenced by exploration and exploitation. The quality of the solution determines the

material's stability, denoted as Mat. The level of material stability corresponds to the worst and best values among the optimal solutions, as defined by Eq. (5).

$$Mat = \begin{bmatrix} Mat_1 \\ Mat_2 \\ \vdots \\ Mat_i \\ \vdots \\ Mat_n \\ Mat_{new1} \\ Mat_{new2} \end{bmatrix}, \quad i = 1, 2, ..., n \tag{5}$$

2.1. Proposed formula for IMGA

In this section, a novel formula is proposed to enhance the performance of the Material Generation Algorithm (MGA). Previously, MGA was introduced as an optimization model based on the combination of different materials at various scales—atomic, nano, micro, or macro—to address optimization problems. While MGA is effective at converging to the global optimum in solving unconstrained problems with relatively few iterations, it struggles with frequency-constrained engineering problems that are highly nonlinear and feature many local optima. This shortcoming arises because MGA's structure limits the production of new materials, resulting in a lack of diversity in responses examined during each iteration. Consequently, MGA often gets trapped in local optima due to repetitive solutions.

Despite offering a novel approach to optimization by mimicking material combination and chemical reaction processes, MGA has several weaknesses. A primary limitation is its propensity to become trapped in local optima, stemming from its reliance on existing material compounds for generating new solutions. This constraint hampers its ability to thoroughly explore the solution space and reduces its effectiveness in finding the global optimum. Additionally, MGA's performance is highly dependent on the initial random population and the probabilistic nature of electron sharing or transferring, which can lead to inconsistencies and variability in results. The computational complexity involved in simulating chemical reactions and stability phases can also be significant, making the algorithm less efficient for larger, more complex problems. Furthermore, MGA's requirement for fine-tuning various parameters, such as the participation coefficient and random number generation, adds to its complexity and can make implementation challenging without extensive domain knowledge. Lastly, although MGA draws inspiration from real-world chemical processes, the simplifications and assumptions in its mathematical modeling may not always accurately represent the true nature of material interactions, potentially limiting its applicability to certain types of optimization problems.

A novel technique known as Random Chaotic (RC) has been employed to enhance convergence speed and strike a balance between exploration and exploitation. Initially, Eq. (6) was applied to regulate ion distribution among various materials, thereby fostering diversity in the subsequent phase where different materials are amalgamated to form new compounds. However, this approach alone does not consistently yield superior outcomes and can sometimes become stuck in local optima. To address this challenge, Eq. (7) is

introduced to generate novel combinations, thereby expanding the pool of potential optimal solutions in each iteration and facilitating exploration across the entire search space to identify global optima.

$$Chaos.PTE = PTE^{k}_{new_1} \times (1 + \beta \times randn) , \quad k = 1, 2, ..., d \tag{6}$$

$$Chaos.Mat = Mat_{new_2} \times (1 + \beta \times randn) , \quad j = 1, 2, ..., l \tag{7}$$

where $Chaos.PTE$ is a new chaotic generated material, β is constant which set to 0.2, *randn* is a random operator.

Developing a Material Generation Algorithm based on Random Chaotic (RC) marks a significant leap in addressing dynamically constrained optimization problems. This approach boasts several advantages that set it apart in the realm of algorithmic optimization. Primarily, by harnessing RC, the algorithm accelerates convergence speed while maintaining a delicate equilibrium between exploration and exploitation. This capability proves indispensable for dynamically constrained problems where conditions and constraints may fluctuate over time. RC's ability to dynamically adjust and generate diverse material compositions using Eq. (6) ensures that the algorithm can effectively adapt to evolving constraints and environmental factors. Additionally, the algorithm's capacity to tackle local optima, as exemplified by Eq. (7), offers a pivotal edge. Through the generation of fresh combinations and expansion of the solution space in each iteration, RC diminishes the risk of becoming ensnared in suboptimal solutions. This proactive approach not only fortifies the algorithm's resilience against local optima but also augments its aptitude for exploration and potential convergence toward global optima.

Moreover, RC's inherent flexibility ensures strong performance across diverse applications, spanning from materials science to engineering and beyond. Its capability to adapt to various problem domains highlights its versatility and relevance in real-world situations characterized by dynamic and evolving constraints. Essentially, the development of a Material Generation Algorithm based on RC represents a notable advancement in optimization techniques. Its proficiency in addressing dynamically constrained problems, alleviating issues with local optima, and consistently delivering robust performance across a wide array of applications positions it as a promising approach for enhancing optimization capabilities across different fields of study and industry applications.

3. DEFINITION OF THE OPTIMIZATION PROBLEM

In a typical optimization problem, an objective function serves as the criterion to identify the optimal solutions among all possible candidates, often expressed in terms of one or more design variables. Essentially, the optimal design is achieved by minimizing this objective function. In this context, cost reduction is the primary goal, influenced by numerous factors that interact in complex ways. While the relationships among these factors are intricate, a reasonable assumption holds that minimizing the weight of the structure correlates with reduced construction costs. Hence, we have selected the total weight of the structure, excluding lumped masses, as our objective function. The design variables encompass nodal

coordinates and the cross-sectional areas of structural members. The objective function, along with design variables, constraints, and penalty functions, are defined through the following equations to formalize this optimization process.

$$F(X) = \sum_{i=1}^{m} A_i \rho_i L_i \tag{8}$$

$$\text{find} \quad X = \{A, N\}, A = \{A_1, A_2, A_3, ..., A_m\} \quad \text{and} \quad N = \{N_1, N_2, N_3, ..., N_n\} \tag{9}$$

$$\begin{cases} g_1(X): f_q \geq f_q^{\min} \\ g_2(X): f_r \leq f_r^{\max} \\ g_3(X): A_i^{\min} \leq A_i \leq A_i^{\max} \\ g_4(X): N_j^{\min} \leq N_j \leq N_j^{\max} \\ \text{where} \;\; i = 1, 2, ..., m; \;\; j = 1, 2, ..., n. \end{cases} \tag{10}$$

$$F(X) = \begin{cases} \text{If there is no violation,} \; F(X) \\ \text{otherwise,} \; F(X) \times F_{Penalty} \end{cases} \tag{11}$$

where A_i, ρ_i, and L_i are the cross-sectional area, density, and length of the i^{th} bar respectively. N_j represents the nodal coordinates (in the directions x_j, y_j, and z_j) of the j^{th} node; and f_q and f_r are respectively the q^{th} and r^{th} natural frequencies. Superscripts *max* and *min* denote the upper and lower allowable limits, respectively. A penalty condition is defined as follows: if there is no violation, the objective function will not be penalized; otherwise, it will be penalized using a penalty function defined as:

$$F_{Penalty} = (1 + \varepsilon_1 \times \psi)^{\varepsilon_2}, \qquad \psi = \sum (\psi_q + \psi_r), \tag{12}$$

$$\psi_q = \left| 1 - \frac{\left| f_q - f_q^{\min} \right|}{f_q^{\min}} \right| \quad \text{and} \quad \psi_r = \left| 1 - \frac{\left| f_r - f_r^{\max} \right|}{f_r^{\max}} \right| \tag{13}$$

where parameters ε_1 and ε_2 are constraint integers determined based on experience. In this study, it is assumed $\varepsilon_1 = \varepsilon_2 = 3$.

4. STRUCTURAL DESIGN PROBLEMS AND DISCUSSIONS

Numerical examples demonstrating the effectiveness of the proposed algorithms in optimizing truss structures are presented. Specifically, the study includes five different truss configurations: a 37-bar, a 52-bar, a 72-bar, a 120-bar, and a 200-bar truss. These structures serve as test cases to evaluate the performance of the proposed algorithm against traditional methods found in existing literature. Additionally, to provide a comprehensive analysis of the results, two key metrics—Standard Deviation (SD) and Number of Function Evaluations (NFE)—are employed. SD assesses the stability of the obtained solutions, while NFE quantifies the computational efficiency of the algorithms. Importantly, each optimization problem is repeated 30 times to ensure robustness and reliability of the findings.

4.1. The 37-bar bridge truss structure

The first numerical example is a 37-bar truss the geometry of which is illustrated in Fig. 1. The design variables include 14 cross-sectional and 5 nodal variables. Thus, this truss considered size and shape optimization simultaneously. The lower and upper allowable cross-sectional areas are 1 and 10 cm^2, respectively, while the lower and upper allowable node variables are 0.1 and 3 m, respectively. The coefficient of elasticity is $E = 2{:}1e11Pa$ and the mass density is $\rho = 7800\ kg/m^3$. Also, the constraints on natural frequencies f_1, f_2, and f_3 are as follows: $f_1 \geq 20$, $f_2 \geq 40$, and $f_3 \geq 60$ Hz. The lumped mass which is neglected in the calculation of the objective function is $m = 10\ kg$, which is applied to the lower nodes of the bridge.

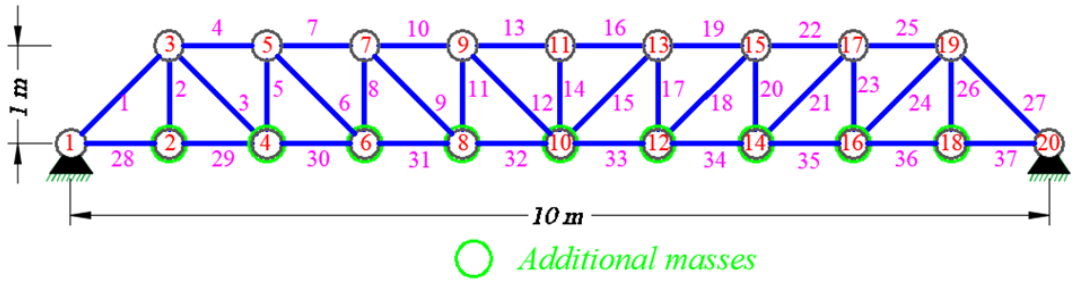

Figure 1: The 37-bar bridge truss structure with additional masses

The optimal results of IMGA and OC [30], GA [31], PSO [32], HS [33], DPSO [35], and SOS [37] are shown in Table 1. The best optimal weight among comparative algorithms 360.024 belongs to IMGA. Also, IMGA with 7,000 has the worst weight and average weight of 363.324 and 360.862 with a standard deviation of 8.17106. In solving this example, IMGA has obtained good answers, but the dispersion of answers around the optimal point is worse than SOS, DPSO, HS, and PSO. The worst optimal response is obtained by GA with a value of 368.84. This shows that the performance of the new generation of metaheuristic algorithms has improved compared to the earlier methods. The frequency results of the first to third modes are presented in Table 2. The convergence history results of IMGA and other methods for the best weight, worst weight, and average weight are plotted in Fig. 6a.

Table 1: Results of IMGA, and other methods for solving the 37-bar truss problem

Design variables	Wang et al. 2004 (OC) [30]	Wei et al. 2005 (GA) [31]	Gomes 2011 (PSO) [32]	Miguel 2012 (HS) [33]	Kaveh and Zolghadr 2014 (DPSO) [35]	Tejani et al. 2016 (SOS) [37]	**This study**
							IMGA
Y_3, Y_{19}	1.2086	1.1998	0.9637	0.8415	0.9482	0.9598	1.0000
Y_5, Y_{17}	1.5788	1.6553	1.3978	1.2409	1.3439	1.3867	1.3569
Y_7, Y_{15}	1.6719	1.9652	1.5929	1.4464	1.5043	1.5698	1.5498
Y_9, Y_{13}	1.7703	2.0737	1.8812	1.5334	1.6350	1.6687	1.6866
Y_{11}	1.8502	2.3050	2.0856	1.5971	1.7182	1.7203	1.7430
A_1, A_{27}	3.2508	2.8932	2.6797	3.2031	2.6208	2.9038	2.9291

A_2, A_{26}	1.2364	1.1201	1.1568	1.1107	1.0397	1.0163	1.0000
A_3, A_{24}	1.0000	1.0000	2.3476	1.1871	1.0464	1.0033	1.0071
A_4, A_{25}	2.5386	1.3655	1.7182	3.3281	2.7163	3.1940	2.7055
A_5, A_{23}	1.3714	1.5962	1.2751	1.4057	1.0252	1.0109	1.0468
A_6, A_{21}	1.3681	1.2642	1.4819	1.0883	1.5081	1.5877	1.2957
A_7, A_{22}	2.4290	1.8254	4.6850	2.1881	2.3750	2.4104	2.5756
A_8, A_{20}	1.6522	2.0009	1.1246	1.2223	1.4498	1.3864	1.3644
A_9, A_{18}	1.8257	1.9526	2.1214	1.7033	1.4499	1.6276	1.5315
A_{10}, A_{19}	2.3022	1.9705	3.8600	3.1885	2.5327	2.3594	2.4859
A_{11}, A_{17}	1.3103	1.8294	2.9817	1.0100	1.2358	1.0293	1.1896
A_{12}, A_{15}	1.4067	1.2358	1.2021	1.4074	1.3528	1.3721	1.3368
A_{13}, A_{16}	2.1896	1.4049	1.2563	2.8499	2.9144	2.0673	2.1529
A_{14}	1.0000	1.0000	3.3276	1.0269	1.0085	1.0000	1.0170
Best (kg)	366.50	368.84	377.20	361.50	360.40	360.865	360.024
Worst	-	-	-	-	-	-	363.324
Mean	NA	NA	381.20	362.04	362.21	364.852	360.862
SD	NA	9.0325	4.26	0.52	1.68	2.9650	8.7106
NFEs	NA	NA	12,500	20,000	6,000	4,000	7,000

Table 2: Natural frequencies (Hz) of the 37-bar bridge truss structure

Natural frequency	Wang et al. 2004 (OC) [30]	Wei et al. 2005 (GA) [31]	Gomes 2011 (PSO) [32]	Miguel 2012 (HS) [33]	Kaveh and Zolghadr 2014 (DPSO) [35]	Tejani et al. 2016 (SOS) [37]	**This study**
							IMGA
f_1	20.0850	20.0013	20.0001	20.0037	20.0194	20.0366	20.0010
f_2	42.0743	40.0305	40.0003	40.0050	40.0113	40.0007	40.0010
f_3	62.9383	60.0000	60.0001	60.0082	60.0082	60.0138	60.0000

4.2. The 52-bar space truss structure

The52-bar truss'sthe top and front views of which are shown in Figure and is considered an optimization problem to examine the relative performance of IMGA. The design variables of this problem include 8 cross-sectional and 5 nodal variables. Therefore, this problem also considered size and shape optimization simultaneously. The minimum and maximum allowable cross-sectional areas are 0.0001 and 0.001 m^2, respectively. The allowable displacement of each node is $\pm 2\,\mathrm{m}$ along the vertical axis. The coefficient of elasticity is $E = 2.1 \times 10^{11}(\mathrm{N/m^2})$ and the mass density is $\rho = 7800(\mathrm{kg/m^3})$. Also, the constraints on natural frequencies f_1 and f_2 are as follows: $f_1 \le 15.916\,\mathrm{Hz}$ and $f_2 \ge 28.649\,\mathrm{Hz}$. The lumped mass which is neglected in the calculation of the objective function is m = 50 kg; this load is applied to the truss at all the free nodes of the dome. As can be seen from Figure b, the truss structure is symmetric about the vertical axis.

The Results of IMGA and Bi-factor [38], NGHA [31], PSO [32], HS [33], FA [33], CSS-BBBC [39] DPSO [35], TLBO [36], and SOS [37] are presented in Table 3. The best optimal weight of IMGA is equal to 193.20, which is placed after TLBO [36] with a very

small difference. IMGA has reached the best optimal answer with 8,000 analyses. As long as TLBO [36] 15,000 analyzes have reached the optimal answer, which is almost spent twice the computational cost. The best optimal weight for Bi-factor [38], NGHA [31], PSO [32], HS [33], FA [33], CSS-BBBC [39] DPSO [35], and SOS [37] respectively 298.00, 236.04, 228.38, 214.94, 197.53, 197.30, 195.35, and 195.49. The Bi-factor does not report any information about the Mean, Standard Deviation, and number of analyses. The frequencies of the first two modes are presented in Table 4. The convergence diagram of IMGA is drawn in Fig. 6b IMGA has converged to the global optimal answer at high speed and after 20 iterations.

Table 3: Comparative results of IMGA and other methods for solving the 52-bar dome truss problem

Design variables	Lin et al. 1982 (Bi-factor) [38]	Wei et al. 2005 (NGHA) [31]	Gomes 2011 (PSO) [32]	Miguel 2012 (HS) [33]	Miguel 2012 (FA) [33]	Kaveh and Zolghadr 2012 (CSS-BBBC) [39]	Kaveh and Zolghadr 2014 (DPSO) [35]	Farshchin et al. 2016 (TLBO) [36]	Tejani et al. 2016 (SOS) [37]	**This study**
										IMGA
Z_A	4.3201	5.8851	5.5344	4.7374	6.4332	5.3310	6.1123	6.0026	5.7624	5.9659
X_B	1.3153	1.7623	2.0885	1.5643	2.2208	2.1340	2.2343	2.2626	2.3239	2.233
Z_B	4.1740	4.4091	3.9283	3.7413	3.9202	3.7190	3.8321	3.7452	3.7379	3.7301
X_F	2.9169	3.4406	4.0255	3.4882	4.0296	3.9350	4.0316	3.9854	3.9842	3.9511
Z_F	3.2676	3.1874	2.4575	2.6274	2.5200	2.5000	2.5036	2.5000	2.5121	2.5014
$A_1 - A_4$	1.00	1.0000	0.3696	1.0085	1.0050	1.0000	1.0001	1.0000	1.0988	1.0000
$A_5 - A_8$	1.33	2.1417	4.1912	1.4999	1.3823	1.3056	1.1397	1.1210	1.0031	1.1307
$A_9 - A_{16}$	1.58	1.4858	1.5123	1.3948	1.2295	1.4230	1.2263	1.2113	1.1956	1.2205
$A_{17} - A_{20}$	1.00	1.4018	1.5620	1.3462	1.2662	1.3851	1.3335	1.4486	1.4563	1.4691
$A_{21} - A_{28}$	1.71	1.9110	1.9154	1.6776	1.4478	1.4226	1.4161	1.4156	1.3773	1.4117
$A_{29} - A_{36}$	1.54	1.0109	1.1315	1.3704	1.0000	1.0000	1.0001	1.0000	1.0055	1.0000
$A_{37} - A_{44}$	2.65	1.4693	1.8233	1.4137	1.5728	1.5562	1.5750	1.5434	1.7397	1.6243
$A_{45} - A_{52}$	2.87	2.1411	1.0904	1.9378	1.4153	1.4485	1.4357	1.4034	1.3084	1.3304
Best (kg)	298.00	236.04	228.38	214.94	197.53	197.30	195.35	193.18	195.49	193.20
Worst	-	-	-	-	-	-	-	-	-	202.04
Mean	NA	NA	234.30	205.61	212.80	NA	198.71	200.30	214.66	197.59
SD	NA	37.462	5.22	12.44	17.98	NA	13.85	15.48	14.14	45.55
NFEs	NA	NA	11,270	20,000	10,000	4,000	6,000	15,000	4,000	8,000

Table 4: Natural frequencies (Hz) of the 52-bar dome truss structure

Natural frequency	Lin et al. 1982 (Bi-factor) [38]	Wei et al. 2005 (NGHA) [31]	Gomes 2011 (PSO) [32]	Miguel 2012 (HS) [33]	Miguel 2012 (FA) [33]	Kaveh and Zolghadr 2012 (CSS-BBBC) [39]	Kaveh and Zolghadr 2014 (DPSO) [35]	Farshchin et al. 2016 (TLBO) [36]	Tejani et al. 2016 (SOS) [37]	**This study**
										IMGA
f_1	15.22	12.81	12.75	12.22	11.31	12.98	11.31	11.46	12.71	11.294
f_2	29.28	28.65	28.64	28.65	28.65	28.64	28.64	28.64	28.65	28.648

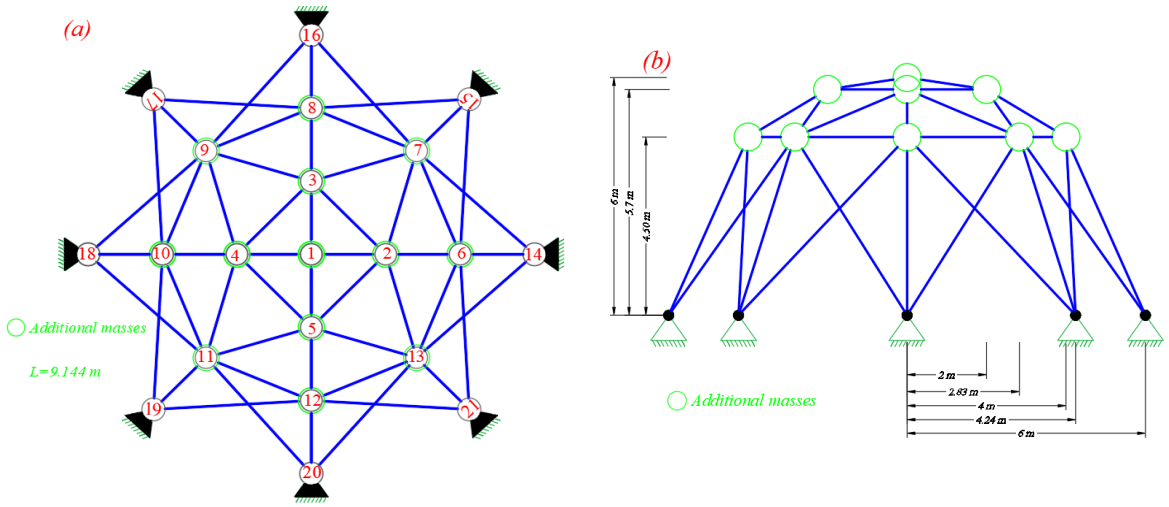

Figure 2: The 52-bar space truss structure with additional masses: (a) top view; (b) side view

4.3. The 72-bar space truss structure

As the third problem, a 72-bar truss is taken as illustrated in Figure . The design variables are cross-sectional areas, which is divided into 16 sets . The minimum and maximum allowable cross-sectional areas are 0.645 and 30 cm^2, respectively. The coefficient of elasticity is $E = 6.98 \times 10^{11} (N/m^2)$ and the mass density is $\rho = 2770$ (kg/m^3). Also, the constraints on natural frequencies f_1 and f_2 are as follows: $f_1 \geq 4\,Hz$ and $f_2 \geq 6\,Hz$. A lumped mass m = 2770 kg, which is neglected in the calculation of the objective function, is added to the truss at nodes 1 to 4.

The results of IMGA and other metaheuristic methods for optimizing the 72-bar structure under frequency constraints are presented in Table 5. The best optimal weights for IMGA, CSS-BBBC [39], CBO [34], TLBO [36], FA [33], PSO [35], and SOS [37] are 324.562, 327.507, 324.7552, 327.568, 327.575, 327.691, 328.81, and 325.558, respectively.The best weight belongs to IMGA and the worst weight belongs to PSO [35]. One of the good features of IMGA is that it can reach the optimal answer with the lowest computational cost. In this example, it has converged to the optimal point with only 6000 analyses. The convergence diagram of IMGA is drawn in Fig. 6c. The frequencies of the first two modes are presented in Table 6.

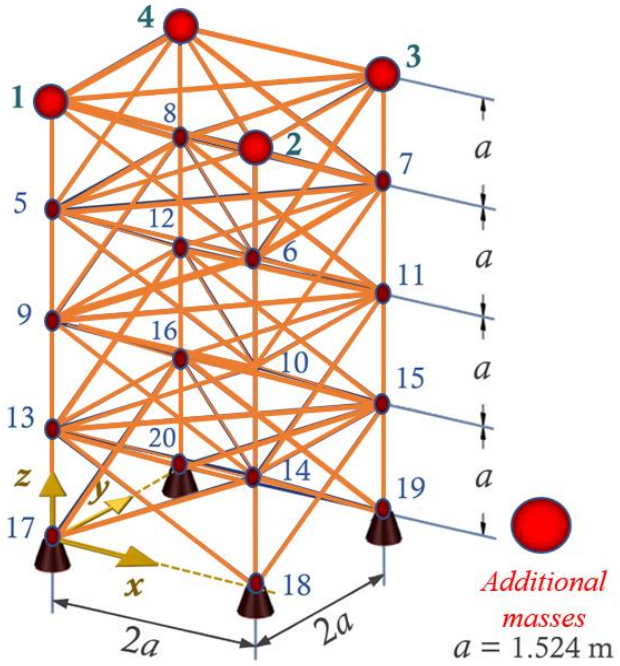

Figure 3: The 72-bar space truss structure with additional masses

Table 5: Comparative results of IMGA, and other methods for solving the 72-bar space truss problem

Design variables	Kaveh and Zolghadr 2012 (CSS-BBBC) [39]	Kaveh and Mahdavi 2014 (CBO) [34]	Farshchin et al. 2016 (TLBO) [36]	Farshchin et al. 2016 (TLBO) [36]	Miguel 2012 (FA) [33]	Kaveh and Zolghadr 2014 (PSO) [35]	Tejani et al. 2016 (SOS) [37]	**This study** **IMGA**
$A_1 – A_4$ (cm^2)	2.854	3.3699	3.5491	3.4188	3.3411	2.9870	3.6957	3.63411
$A_5 – A_{12}$ (cm^2)	8.301	7.3428	7.9676	7.9263	7.7587	7.8490	7.1779	7.94525
$A_{13} – A_{16}$ (cm^2)	0.645	0.6468	0.6450	0.6450	0.6450	0.6450	0.6450	0.6450
$A_{17} – A_{18}$ (cm^2)	0.645	0.6457	0.6450	0.6450	0.6450	0.6450	0.6569	0.64718
$A_{19} – A_{22}$ (cm^2)	8.202	8.0056	8.1532	8.0143	9.0202	8.7650	7.7017	7.48083
$A_{23} – A_{30}$ (cm^2)	7.043	8.0185	7.9667	7.9603	8.2567	8.1530	7.9509	7.83967
$A_{31} – A_{34}$ (cm^2)	0.645	0.6458	0.6450	0.6450	0.6450	0.6450	0.6450	0.64517
$A_{35} – A_{36}$ (cm^2)	0.645	0.6457	0.6450	0.6450	0.6450	0.6450	0.6450	0.64521
$A_{37} – A_{40}$ (cm^2)	16.328	12.4585	12.9272	12.7903	12.045	13.450	12.3994	13.2464
$A_{41} – A_{48}$ (cm^2)	8.299	8.1211	8.1226	8.1013	8.0401	8.0730	8.6121	8.01889
$A_{49} – A_{52}$ (cm^2)	0.645	0.6460	0.6452	0.6450	0.6450	0.6450	0.6450	0.67388
$A_{53} – A_{54}$ (cm^2)	0.645	0.6459	0.6450	0.6473	0.6450	0.6450	0.6450	0.64723
$A_{55} – A_{58}$ (cm^2)	15.048	17.3636	17.0524	17.4615	17.380	16.684	17.4827	16.9046
$A_{59} – A_{66}$ (cm^2)	8.268	8.3371	8.0618	8.1304	8.0561	8.0561	8.1502	7.95071
$A_{67} – A_{70}$ (cm^2)	0.645	0.6460	0.6450	0.6450	0.6450	0.6450	0.6740	0.66917
$A_{71} – A_{72}$ (cm^2)	0.645	0.6476	0.6450	0.6451	0.6450	0.6450	0.6550	0.65286
Best (kg)	327.507	324.7552	327.568	327.575	327.691	328.81	325.558	324.562
Worst	-	-	-	-	-	-	-	328.182
Mean	NA	330.4154	328.684	327.693	329.890	332.24	331.122	325.705
SD	NA	7.7063	0.73	0.1250	2.59	4.23	4.227	11.933
NFEs	4,000	6,000	15,000	15,000	10,000	42,840	4,000	6,000

Table 6: Natural frequencies (Hz) of the 72-bar space truss problem

Natural frequency	Kaveh and Zolghadr 2012 (CSS-BBBC) [39]	Kaveh and Mahdavi 2014 (CBO) [34]	Farshchin et al. 2016 (TLBO) [36]	Farshchin et al. 2016 (TLBO) [36]	Miguel 2012 (FA) [33]	Kaveh and Zolghadr 2014 (PSO) [35]	Tejani et al. 2016 (SOS) [37]	**This study**
								IMGA
f_1	4.000	4.000	4.000	4.000	4.000	3.9999	4.0023	4.0000
f_2	6.004	6.000	6.000	6.000	6.000	3.9999	4.0020	4.0000

4.4. The 120-bar dome structure

In this section, a 120-bar truss, depicted in Fig. 4, is considered an optimization problem to test the relative capability of IMGA. The truss bars are grouped into 7 by seeing symmetry on the z-axis. Thus, the design variables of this problem include 7 cross-sectional variables. The minimum and maximum allowable cross-sectional areas are 0.0001 and 0.01293 m2, respectively. The coefficient of elasticity is $E = 2.1 \times 10^{11} (\mathrm{N/m^2})$and the mass density is ρ=7,971.81 (kg m^3). Also, the constraints on natural frequencies f1 and f2 aref_1≤9 "Hz" and f_2≥11 "Hz". The lumped masses which are neglected in the calculation of the objective function are 3000 kg at node-1500 kg at nodes-2 to nodes-13, and 100 kg at the rest of the free nodes.

Results of optimal design of 120-bar structure with frequency constraints for IMGA, PSO [35], DPSO [35], CSS [39], CSS-BBBC [39], CBO [34], SOS [37], and SOS-ABFI [37]] is presented in Table 7. IMGA has performed best in solving this 3D structure. IMGA has obtained the best results with 10000 analyses, Best=8708.80, Worst=8756.36, Mean=8721.07, and SD=1.42. The convergence diagram of IMGA is drawn in Figure 6d. The proposed algorithm has converged to the optimal answer with high speed after 20 iterations. The frequencies of the first five modes are presented in Table 8.

Table 7: Comparative results of IMGA and other methods for solving the 120-bar dome truss problem

Design variables	Kaveh and Zolghadr 2014 (PSO) [35]	Kaveh and Zolghadr 2014 (DPSO) [35]	Kaveh and Zolghadr 2012 (CSS) [39]	Kaveh and Zolghadr 2012 (CSS-BBBC) [39]	Kaveh and Mahdavi 2014 (CBO) [34]	Tejani et al. 2016 (SOS) [37]	Tejani et al. 2016 (SOS-ABF1) [37]	**This study**
								IMGA
G_1 (cm^2)	23.494	19.607	21.710	17.478	19.691	19.520	19.544	19.5265
G_2 (cm^2)	32.976	41.290	40.862	49.076	41.142	40.848	40.948	40.446
G_3 (cm^2)	11.492	11.136	9.048	12.365	11.155	10.322	10.448	10.8192
G_4 (cm^2)	24.839	21.025	19.673	21.979	21.320	20.927	21.046	21.0474
G_5 (cm^2)	9.964	10.060	8.336	11.190	9.833	9.655	9.504	9.68791
G_6 (cm^2)	12.039	12.758	16.120	12.590	12.852	12.112	11.936	11.4599
G_7 (cm^2)	14.249	15.414	18.976	13.585	15.160	15.0313	14.942	14.9898
Best (kg)	9171.93	8890.48	9204.51	9046.34	8889.13	8713.30	8712.11	8708.80
Worst	-	-	-	-	-	-	-	8756.36
Mean	9251.84	8895.99	-	-	8891.25	8735.34	8727.42	8721.07
SD	89.38	4.26	-	-	1.79	17.90	16.55	1.42
NFEs	6,000	6,000	4,000	4,000	6,000	4,000	4,000	10,000

Table 8: Natural frequencies (Hz) of the 120-bar dome truss problem

Natural frequency	Kaveh and Zolghadr 2014 (PSO) [35]	Kaveh and Zolghadr 2014 (DPSO) [35]	Kaveh and Zolghadr 2012 (CSS) [39]	Kaveh and Zolghadr 2012 (CSS-BBBC) [39]	Kaveh and Mahdavi 2014 (CBO) [34]	Tejani et al. 2016 (SOS) [37]	Tejani et al. 2016 (SOS-ABF1) [37]	**This study** **IMGA**
f_1	9.000	9.000	9.002	9.000	9.000	9.000	9.001	9.0000
f_2	11.000	11.000	11.002	11.007	11.000	11.000	11.000	11.000
f_3	11.005	11.005	11.006	11.018	11.000	11.000	11.000	11.000
f_4	11.013	11.012	11.015	11.026	11.009	11.004	11.001	11.000
f_5	11.042	11.047	11.045	11.048	11.049	11.071	11.067	11.066

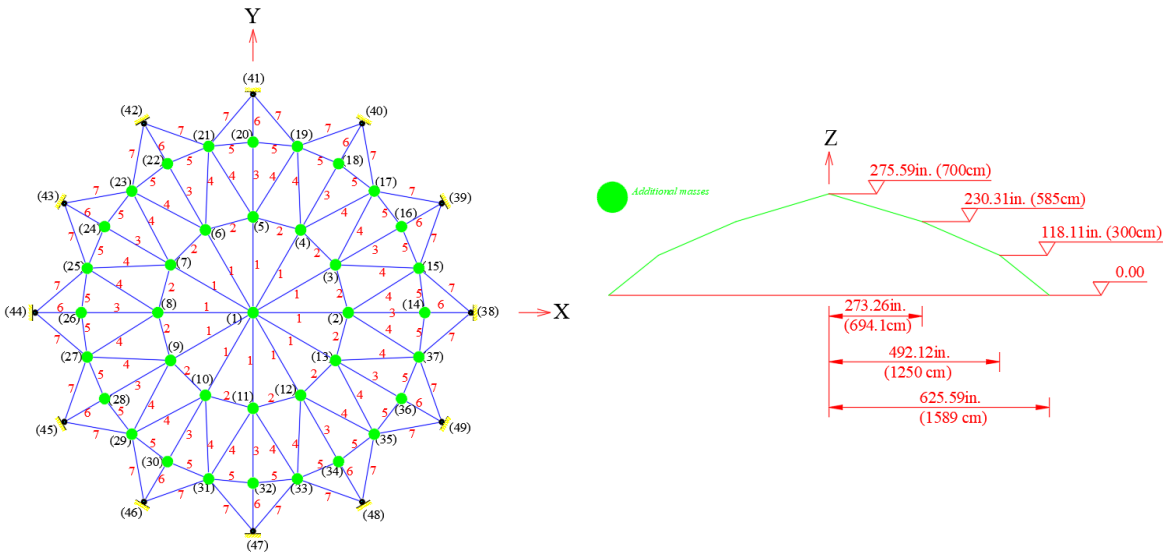

Figure 4: The 120-bar dome structure with additional masses

4.5. The 200-bar planar truss structure

This problem presented in this study to examine the capabilities of IMPA deals with a 200-bar truss as depicted in Figure . The design variables are cross-sectional areas, classified into 29 sets as listed in Table 9, where the minimum and maximum allowable cross-sectional areas are 0.1 and 30 cm^2, respectively. The coefficient of elasticity is $E = 2.1\times10^{11}(N/m^2)$ and the mass density is $\rho = 7860\ (kg/m^3)$. The constraints on natural frequencies f_1, f_2, and f_3 are as follows: $f_1 \geq 5$, $f_2 \geq 10$, and $f_3 \geq 15\,Hz$. The lumped mass m = 100 kg, which is neglected in the calculation of the objective function, is added to the top of the truss at nodes 1 to 5.

The results of IMGA and other metaheuristic methods for solving the structure of 200 members are presented in Table 10. IMGA has obtained optimal results with 25,000 analysis including Best=2166.91, Worst=2210.74, Mean=2180.81, and SD=1.267. The 29 optimal cross-sections designed by IMGA are shown in Table 10 respectively. In this example, TLBO [36] and OM-GSA [40] were ranked first and second, respectively, and IMGA was

ranked third. Investigations show that the optimal results of IMGA have a suitable level of confidence. The convergence diagram of IMGA for iteration is shown in Fig. 6e. Based on the IMGA convergence diagram, it has converged with a high speed to the optimal response. The results of the first, second, and third frequencies are presented in Table 11.

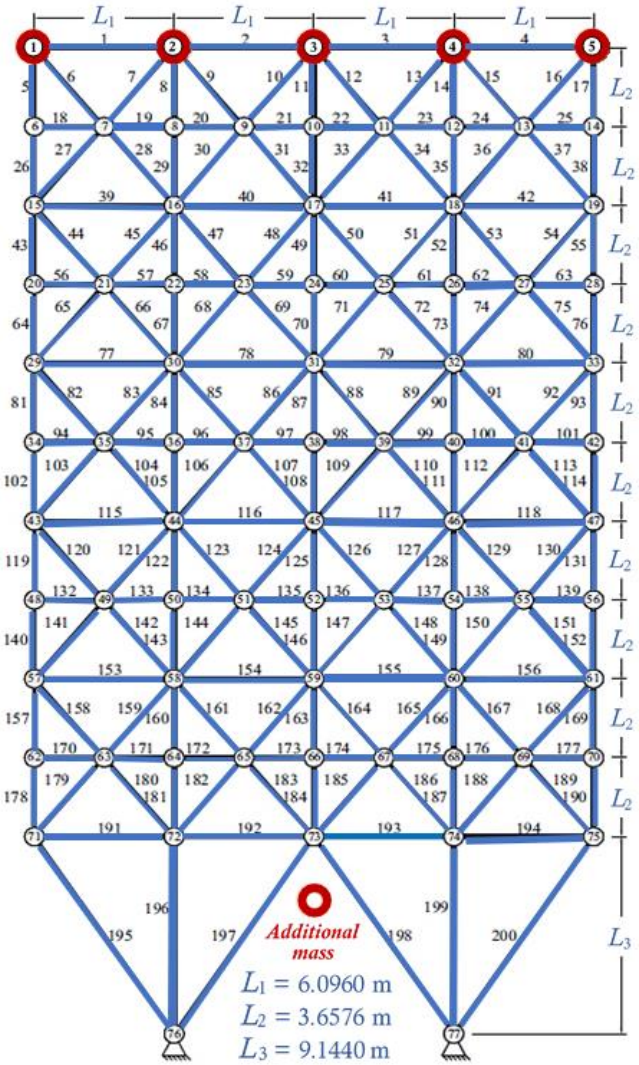

Figure 5: The 200-bar planar truss structure with additional masses

Table 9: Element grouping for the 200-bar truss structure

Group	Element's number	Group	Element's number
G_1	A_1, A_2, A_3,A_4	G_{16}	A_{82}, A_{83}, A_{85}, A_{86}, A_{88},A_{89}, A_{91}, A_{92}, A_{103}, A_{104}, A_{106}, A_{107}, A_{109}, A_{110}, A_{112}, A_{113}
G_2	A_5, A_8, A_{11}, A_{14},A_{17}	G_{17}	A_{115}, A_{116}, A_{117}, A_{118}
G_3	A_{19}, A_{20}, A_{21}, A_{22}, A_{23},A_{24}	G_{18}	A_{119}, A_{122}, A_{125}, A_{128}, A_{131}
G_4	A_{18}, A_{25}, A_{56}, A_{63}, A_{94}, A_{101}, A_{132}, A_{139}, A_{170}, A_{177}	G_{19}	A_{133}, A_{134}, A_{135}, A_{136}, A_{137}, A_{138}
G_5	A_{26}, A_{29}, A_{32}, A_{35}, A_{38}	G_{20}	A_{140}, A_{143}, A_{146}, A_{149}, A_{152}
G_6	A_6, A_7, A_9,A_{10}, A_{12}, A_{13}, A_{15}, A_{16}, A_{27}, A_{28}, A_{30}, A_{31}, A_{33}, A_{34}, A_{36},A_{37}	G_{21}	A_{120}, A_{121}, A_{123}, A_{124}, A_{126}, A_{127}, A_{129},A_{130}, A141, A142, A_{44}, A_{145}, A_{147}, A_{148}, A_{150}, A_{151}
G_7	A_{39}, A_{40}, A_{41}, A_{42}	G_{22}	A_{153}, A_{154}, A_{155}, A_{156}
G_8	A_{43}, A_{46}, A_{49}, A_{52}, A_{55}	G_{23}	A_{157}, A_{160}, A_{163}, A_{166}, A_{169}
G_9	A_{57}, A_{58}, A_{59}, A_{60},A_{61}, A_{62}	G_{24}	A_{171}, A_{172}, A_{173}, A_{174}, A_{175}, A_{176}
G_{10}	A_{64}, A_{67}, A_{70}, A_{73}, A_{76}	G_{25}	A_{178}, A_{181}, A_{184}, A_{187}, A_{190}
G_{11}	A_{44}, A_{45}, A_{47}, A_{48}, A_{50}, A_{51}, A_{53}, A_{54}, A_{65}, A_{66}, A_{68}, A_{69}, A_{71}, A_{72}, A_{74}, A_{75}	G_{26}	A_{158}, A_{159}, A_{161},A_{162}, A_{164}, A_{165}, A_{167}, A_{168}, A_{179}, A_{180}, A_{182}, A_{183}, A_{185}, A_{186}, A_{188}, A_{189}
G_{12}	A_{77},A_{78}, A_{79}, A_{80}	G_{27}	A_{191}, A_{192}, A_{193}, A_{194}
G_{13}	A_{81}, A_{84}, A_{87}, A_{90}, A_{93}	G_{28}	A_{195}, A_{197}, A_{198}, A_{20}0
G_{14}	A_{95},A_{96}, A_{97}, A_{98}, A_{99}, A_{100}	G_{29}	A_{196}, A_{199}
G_{15}	A_{102}, A_{105}, A_{108}, A_{111}, A_{114}		

Table 10 Comparative results of IMGA, and other methods for solving the 200-bar planar truss structure problem

Design variables	Khatibinia and Naseralavi 2014 (OM-GSA) [40]	Kaveh and Mahdavi 2015 (CBO) [41]	Kaveh and Mahdavi 2015 (2D-CBO) [41]	Farshchin al. 2016 (TLBO) [36]	et Farshchin et al. 2016a (MC-TLBO) [36]	Mortazavi 2021 (CSS) [42]	Kaveh and Zolghadr 2014 (PSO) [35]	Tejani et al. 2016 (SOS) [37]	**This study**
									IMGA
G_1 (cm^2)	0.289	0.3268	0.4460	0.3030	0.3067	1.2439	2.4662	0.4781	0.259844
G_2 (cm^2)	0.486	0.4502	0.4556	0.4479	0.4450	1.1438	0.1000	0.4481	0.500074
G_3 (cm^2)	0.100	0.1000	0.1519	0.1001	0.1000	0.3769	0.1000	0.1049	0.100391
G_4 (cm^2)	0.100	0.1000	0.1000	0.1000	0.1001	0.1494	0.1000	0.1045	0.100026
G_5 (cm^2)	0.499	0.7125	0.4723	0.5124	0.5077	0.4835	0.1000	0.4875	0.614989
G_6 (cm^2)	0.804	0.8029	0.7543	0.8205	0.8241	0.8103	2.8260	0.9353	0.798391
G_7 (cm^2)	0.103	0.1028	0.1024	0.1000	0.1001	0.4364	0.1000	0.1200	0.102102
G_8 (cm^2)	1.377	1.4877	1.4924	1.4499	1.4367	1.4554	4.6937	1.3236	1.47936
G_9 (cm^2)	0.100	0.1000	0.1000	0.1001	0.1000	1.0103	0.1000	0.1015	0.100215
G_{10} (cm^2)	1.554	1.0998	1.6060	1.5955	1.5787	2.1382	1.7291	1.4827	1.4310
G_{11} (cm^2)	1.151	0.8766	1.2098	1.1556	1.1587	0.8583	1.8842	1.1384	1.18667
G_{12} (cm^2)	0.131	0.1229	0.1061	0.1242	0.1000	1.2718	0.1000	0.1020	0.100153
G_{13} (cm^2)	3.028	2.9058	3.0909	2.9753	2.9573	3.0807	3.7185	2.9943	3.07946
G_{14} (cm^2)	0.101	0.1000	0.7916	0.1000	0.1000	0.2677	0.1000	0.1562	0.103418
G_{15} (cm^2)	3.261	3.9952	3.6095	3.2553	3.2569	4.2403	2.3450	3.4330	3.1657
G_{16} (cm^2)	1.612	1.7175	1.4999	1.5762	1.5733	2.0098	0.9164	1.6816	1.55462
G_{17} (cm^2)	0.209	0.1000	0.1000	0.2680	0.2675	1.5956	0.1000	0.1026	0.170547
G_{18} (cm^2)	5.020	5.9423	5.2951	5.0692	5.0867	6.2338	7.1603	5.0739	5.13813
G_{19} (cm^2)	0.133	0.1102	0.1000	0.1000	0.1004	2.5793	30.000	0.1068	0.148292
G_{20} (cm^2)	5.453	5.8959	4.5288	5.4281	5.4551	3.0520	6.1670	6.0176	5.25655
G_{21} (cm^2)	2.113	2.1858	2.2178	2.0942	2.0998	1.8121	3.1906	2.0340	2.13664
G_{22} (cm^2)	0.723	0.5249	0.7571	0.6985	0.7156	1.2986	0.2150	0.6595	0.751744
G_{23} (cm^2)	7.724	7.2676	7.7999	7.6663	7.6425	5.8810	18.1871	6.9003	8.11257
G_{24} (cm^2)	0.182	0.1278	0.3506	0.1008	0.1049	0.2324	0.1000	0.2020	0.172092
G_{25} (cm^2)	7.971	7.8865	7.8943	7.9899	7.9352	7.7536	30.000	6.8356	8.06052
G_{26} (cm^2)	2.996	2.8407	2.8097	2.8084	2.8262	2.6871	2.0233	2.6644	2.85462
G_{27} (cm^2)	10.206	11.7849	10.4220	10.4661	10.4388	12.5094	16.061	12.1430	9.83976
G_{28} (cm^2)	20.699	22.7014	21.2576	21.2466	21.2125	29.5704	30.000	22.2484	20.6425
G_{29} (cm^2)	11.555	7.8840	11.9061	10.7340	10.8347	8.2910	30.000	8.9378	12.9205

Best (kg)	2158.64	2203.21	2189.08	2156.54	2156.63	2259.86	3987.61	2180.32	2166.91
Worst	-	-	-	-	-	-	-	-	2210.74
Mean	2189.58	2481.49	2308.44	2157.54	2157.44	NA	5027.78	2303.30	2180.81
SD	1.586	250.825	132.514	1.545	0.528	NA	708.95	83.589	1.267
NFEs	15,000	10,000	10,000	23,000	23,000	10,000	20,000	10,000	25,000

Table 11: Comparative results of IMGA and other methods for solving the 200-bar planar truss structure problem

No. frequency	Khatibinia and Naseralavi 2014 (OM-GSA) [40]	Kaveh and Mahdavi 2015 (CBO) [41]	Kaveh and Mahdavi 2015 (2D-CBO) [41]	Farshchin et al. 2016 (TLBO) [36]	Farshchin et al. 2016a (MC-TLBO) [36]	Mortazavi 2021 (CSS) [42]	Kaveh and Zolghadr 2014 (PSO) [35]	Tejani et al. 2016 (SOS) [37]	**This study**
									IMGA
f_1	NA	5.0010	5.0016	5.0000	5.0000	5.0000	5.0650	5.0001	5.000
f_2	NA	12.5247	13.3868	12.2171	12.2306	15.9610	13.1800	13.4306	11.971
f_3	NA	15.1845	15.1981	15.0380	15.0259	16.4070	16.0970	15.2645	15.101

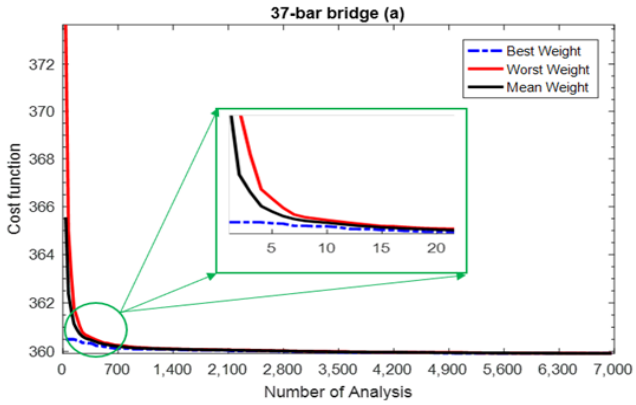

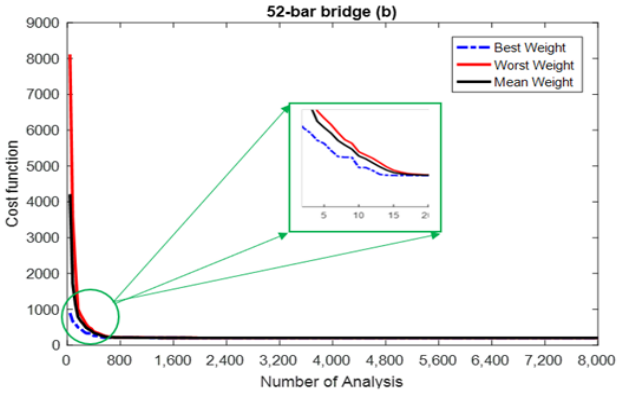

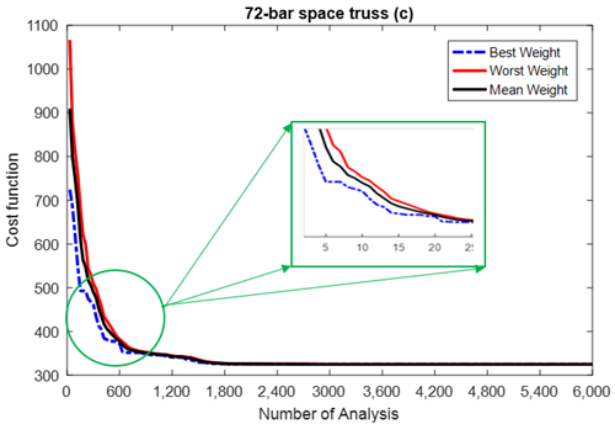

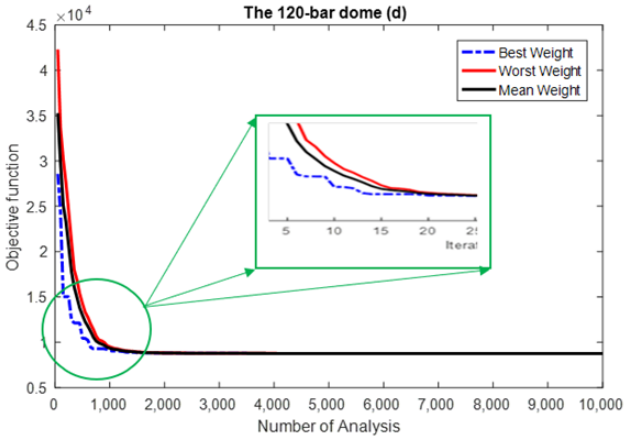

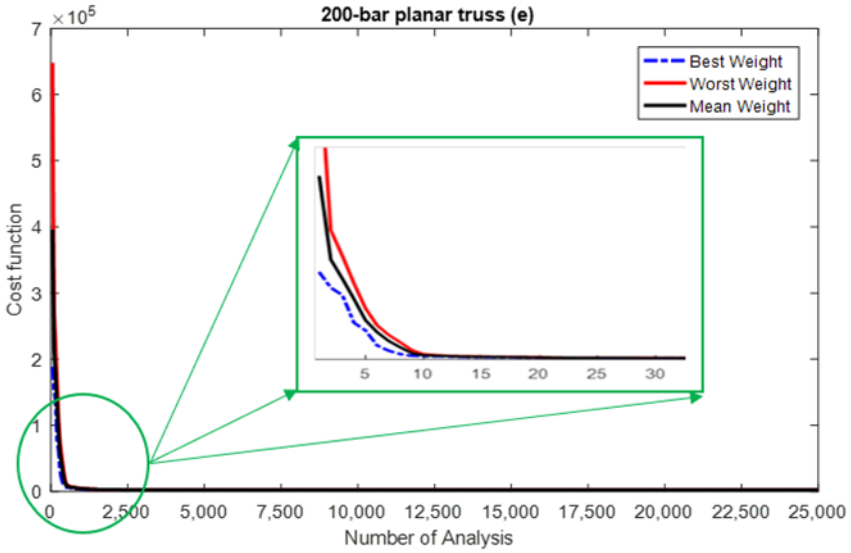

Fig. 6. Convergence history: (a) 37-bar bridge, (b) 52-bar bridge, (c) 72-bar space truss, (d) The 120-bar dome, (e) 200-bar planar truss

5. CONCLUSION

In this study, we introduced the Improved Material Generation Algorithm (IMGA), a metaheuristic approach tailored for addressing engineering problems characterized by dynamic constraints. IMGA draws inspiration from chemical processes wherein materials are combined to create new compounds with enhanced stability and energy levels. The fundamental unit in this algorithm, akin to a chemical element, represents a structure that remains unchanged throughout the optimization process. However, IMGA leverages properties at atomic, nano, and macro scales to refine performance or effect changes, classifying materials based on their distinct attributes. Chemical properties are modified through electron transfers or sharing among atoms, forming the basis for IMGA's optimization strategy, integrating concepts of compounds, reactions, and stability.

This paper extends IMGA by incorporating a novel technique known as Random Chaotic (RC), aimed at accelerating convergence and achieving a balanced approach between exploration and exploitation. RC injects variability into the algorithm's search process, fostering exploration of diverse solutions while exploiting promising paths towards optimization. To assess IMGA's efficacy, we applied it to optimize various complex structures including a 37-bar truss bridge, a 52-bar dome, and 72-bar, 120-bar, and 200-bar planar configurations under frequency constraints. Comparative analysis with other metaheuristic methods demonstrates IMGA's superior performance, particularly in solving nonlinear problems effectively. The findings illustrate IMGA's robustness and versatility in handling challenging optimization tasks, suggesting its potential for applications requiring high computational precision and flexibility. IMGA not only excels in optimizing structures under dynamic constraints but also showcases adaptability to increasingly complex problem

domains. This adaptability is crucial in real-world scenarios where engineering solutions must evolve in response to changing conditions and constraints.

Furthermore, the integration of RC into IMGA significantly enhances its practical utility by improving convergence speed and ensuring a more comprehensive exploration of the solution space. By balancing exploration and exploitation, RC enables IMGA to efficiently navigate complex optimization landscapes, thereby achieving competitive solutions that outperform conventional methods in terms of accuracy and computational efficiency. In conclusion, the development and refinement of IMGA, augmented by the introduction of RC, represent substantial advancements in the realm of metaheuristic optimization. This study not only validates IMGA's effectiveness through empirical testing on diverse structural optimization problems but also underscores its potential for broader applications across engineering disciplines. As computational capabilities continue to evolve, IMGA stands poised to contribute significantly to advancing optimization techniques, offering a promising avenue for future research and practical implementation in complex engineering scenarios.

REFERENCES

1. Pulluri H., Naresh R., Sharma V. A new colliding bodies optimization for solving optimal power flow problem in power system. *2016 IEEE 6th Int Conf Power Syst (ICPS).* IEEE; 2016. https://doi.org/10.1109/ICPES.2016.7584138.
2. Mirjalili S., Mirjalili S. M., Hatamlou A. Multi-Verse Optimizer: A nature-inspired algorithm for global optimization. *Neural Comput Appl.* 2016; **27**(2):495–513. https://doi.org/10.1007/s00521-015-1870-7.
3. Abualigah L., Diabat A., Mirjalili S., Abd Elaziz M., Gandomi A. H. The Arithmetic Optimization Algorithm. *Comput Methods Appl Mech Eng.* 2021; **376**:113609. https://doi.org/10.1016/j.cma.2020.113609.
4. Faramarzi A., Heidarinejad M., Stephens B., Mirjalili S. Equilibrium optimizer: A novel optimization algorithm. *Knowl Based Syst.* 2019; **191**:105190. https://doi.org/10.1016/j.knosys.2019.105190.
5. Goodarzimehr V., Shojaee S., Hamzehei-Javaran S., Talatahari S. Special Relativity Search: A novel metaheuristic method based on special relativity physics. *Knowl Based Syst.* 2022; **109484**. https://doi.org/10.1016/j.knosys.2022.109484.
6. Bayzidi H., Talatahari S., Saraee M., Lamarche C. P. Social network search for solving engineering optimization problems. *Comput Intell Neurosci.* 2021. https://doi.org/10.1155/2021/8548639.
7. Yang Y., Chen H., Heidari A. A., Gandomi A. H. Hunger games search: Visions, conception, implementation, deep analysis, perspectives, and towards performance shifts. *Expert Syst Appl.* 2021; **177**:114864. https://doi.org/10.1016/j.eswa.2021.114864.
8. Wang G. G. Moth search algorithm: A bio-inspired metaheuristic algorithm for global optimization problems. *Memet Comput.* 2018; **10**:151–64. https://doi.org/10.1007/s12293-016-0212-3.
9. Heidari A. A., Mirjalili S., Faris H., Aljarah I., Mafarja M., Chen H. Harris hawks optimization: Algorithm and applications. *Future Gener Comput Syst.* 2019; **97**:849-72. https://doi.org/10.1016/j.future.2019.02.028.

10. Wang G. G., Deb S., Cui Z. Monarch butterfly optimization. *Neural Comput Appl.* 2019; **31**:1995–2014. https://doi.org/10.1016/j.eswa.2020.114418.
11. Li S., Chen H., Wang M., Heidari A. A., Mirjalili S. Slime mould algorithm: A new method for stochastic optimization. *Future Gener Comput Syst.* 2020; **111**:300-23. https://doi.org/10.1016/j.future.2020.03.055.
12. Chen Y., Yan J., Feng J., Sareh P. Particle Swarm Optimization-Based Metaheuristic Design Generation of Non-Trivial Flat-Foldable Origami Tessellations With Degree-4 Vertices. *ASME J Mech Des.* 2021; **143**(1):011703. https://doi.org/10.1115/1.4047437.
13. Abualigah L., Elaziz M. A., Sumari P., Geem Z. W., Gandomi A. H. Reptile Search Algorithm (RSA): A nature-inspired meta-heuristic optimizer. *Expert Syst Appl.* 2022; **191**:116158. https://doi.org/10.1016/j.eswa.2021.116158.
14. Tu J., Chen H., Wang M., et al. The Colony Predation Algorithm. *J Bionic Eng.* 2021; **18**:674–710. https://doi.org/10.1007/s42235-021-0050-y.
15. Azizi M., Talatahari S., Gandomi A. H. Fire Hawk Optimizer: A novel metaheuristic algorithm. *Artif Intell Rev.* 2022; 1–77. https://doi.org/10.1007/s10462-022-10173-w.
16. Talatahari S., Azizi M., Tolouei M., Talatahari B., Sareh P. Crystal Structure Algorithm (CryStAl): A Metaheuristic Optimization Method. *IEEE Access.* 2021; **9**:71244-61. https://doi.org/10.1109/ACCESS.2021.3079161.
17. Javidi A., Salajegheh E., Salajegheh J. Enhanced crow search algorithm for optimum design of structures. *Appl Soft Comput.* 2019; **77**:274–89. https://doi.org/10.1016/j.asoc.2019.01.026.
18. Jafari M., Salajegheh E., Salajegheh J. An efficient hybrid of elephant herding optimization and cultural algorithm for optimal design of trusses. *Eng Comput.* 2019; **35**(3):781–801. https://doi.org/10.1007/s00366-018-0631-5.
19. Cao H., Qian X., Chen Z., Zhu H. Enhanced particle swarm optimization for size and shape optimization of truss structures. *Eng Optim.* 2017; **49**(11):1939–56. https://doi.org/10.1080/0305215X.2016.1273912.
20. Kaveh A., Zakian P. Improved GWO algorithm for optimal design of truss structures. *Eng Comput.* 2018; **34**(4):685–707. https://doi.org/10.1007/s00366-017-0567-1.
21. Degertekin S. O., Lamberti L., Hayalioglu M. S. Heat transfer search algorithm for sizing optimization of truss structures. *Lat Am J Solids Struct.* 2017; **14**(3):373–97. https://doi.org/10.1590/1679-78253297.
22. Kaveh A., Khodadadi N., Azar B. F., Talatahari S. Optimal design of large-scale frames with an advanced charged system search algorithm using box-shaped sections. *Eng Comput.* 2020; **37**:1–21. https://doi.org/10.1007/s00366-020-00955-7.
23. Lee K. S., Geem Z. W. A new structural optimization method based on the harmony search algorithm. *Comput Struct.* 2004; **82**:781–98. https://doi.org/10.1016/j.compstruc.2004.01.002.
24. Degertekin S. O., Tutar H., Lamberti L. School-based optimization for performance-based optimum seismic design of steel frames. *Eng Comput.* 2020; **37**(4):1–15. https://doi.org/10.1007/s00366-020-00993-1.
25. Goodarzimehr V., Omidinasab F., Taghizadieh N. Optimum design of space structures using hybrid particle swarm optimization and genetic algorithm. *World J Eng.* 2022. https://doi.org/10.1108/WJE-05-2021-0279.
26. Goodarzimehr V., Topal U., Bohlooly Fotovat M. Optimal frequency of stiffened piezolaminated composite plates implementing a hybrid special relativity search and hill

climbing optimization algorithm. *J Appl Comput Mech.* 2025. https://doi.org/10.22055/jacm.2024.47914.4837.
27. Topal U., Goodarzimehr V., Bardhan A., Vo-Duy T., Shojaee S. Maximization of the fundamental frequency of the FG-CNTRC quadrilateral plates using a new hybrid PSOG algorithm. *Compos Struct.* 2022; **295**:115823. https://doi.org/10.1016/j.compstruct.2022.115823.
28. Talatahari S., Goodarzimehr V., Shojaee S. Symbiotic organism search and harmony search algorithms for discrete optimization of structures. *Int J Optim Civ Eng.* 2021; **11**(2):177-194. http://ijoce.iust.ac.ir/article-1-471-en.html.
29. Goodarzimehr V., Topal U., Bohlooly M. A novel approach for buckling optimization of stiffened piezolaminated composite plates. *J Compos Mater*. 2024; **58**:2975–91. https://doi.org/10.1177/00219983241288569.
30. Wang D., Zhang W. H., Jiang J. S. Truss optimization on shape and sizing with frequency constraints. *AIAA J.* 2004. **42**(3):622–30. https://doi.org/10.1016/j.jsv.2014.07.027.
31. Wei L., Mei Z., Guangming W., Guang M. Truss optimization on shape and sizing with frequency constraints based on genetic algorithm. *Comput Mech.* 2005. **35**:361–368. https://doi.org/10.1007/s00466-004-0623-8.
32. Gomes H. M. Truss optimization with dynamic constraints using a particle swarm algorithm. *Expert Syst Appl.* 2011. **38(1)**:957–968. https://doi.org/10.1016/j.eswa.2010.07.086.
33. Miguel L. F. F. Shape and size optimization of truss structures considering dynamic constraints through modern metaheuristic algorithms. *Expert Syst Appl.* 2012. **39(10)**:9458–9467. https://doi.org/10.1016/j.eswa.2012.02.113.
34. Kaveh A., Mahdavi V. R. Colliding-bodies optimization for truss optimization with multiple frequency constraints. *J Comput Civ Eng.* 2014. **11**:1–10. https://doi.org/10.1061/(ASCE)CP.1943-5487.0000402.
35. Kaveh A., Zolghadr A. Democratic PSO for truss layout and size optimization with frequency constraints. *Comput Struct.* 2014. **130**:10–21. https://doi.org/10.1016/j.compstruc.2013.09.002.
36. Farshchin M., Camp C. V., Maniat M. Multi-class teaching–learning-based optimization for truss design with frequency constraints. *Eng Struct.* 2016; **106**:355–69. https://doi.org/10.1016/j.engstruct.2015.10.039.
37. Tejani G. G., Savsani V. J., Patel V. K. Adaptive symbiotic organisms search (SOS) algorithm for structural design optimization. *J Comput Des Eng.* 2016; **3**(3)**:**226–49. https://doi.org/10.1016/j.jcde.2016.02.003.
38. Lin J. H., Che W. Y., Yu Y. S. Structural optimization on geometrical configuration and element sizing with static and dynamic constraints. *Comput Struct.* 1982; **15**:507–15. https://doi.org/10.1016/0045-7949(82)90002-5.
39. Kaveh A., Zolghadr A. Truss optimization with natural frequency constraints using a hybridized CSS-BBBC algorithm with trap recognition capability. *Comput Struct.* 2012; 102–103:14–27. https://doi.org/10.1016/j.compstruc.2012.03.016.
40. Khatibinia M., Naseralavi S. Truss optimization on shape and sizing with frequency constraints based on orthogonal multi-gravitational search algorithm. *J Sound Vib.* 2014; **333**(24):6349–69. https://doi.org/10.1016/j.jsv.2014.07.027.
41. Kaveh A., Mahdavi V. R. Two-Dimensional colliding bodies algorithm for optimal design of truss structures. *Adv Eng Softw.* 2015; **83**:70–79. https://doi.org/10.1016/j.advengsoft.2015.01.007.

42. Mortazavi A. Size and layout optimization of truss structures with dynamic constraints using the interactive fuzzy search algorithm. *Eng Optim.* 2021; **53**(3):369–91. https://doi.org/10.1080/0305215X.2020.1726341.
43. Goodarzimehr V., Shojaee S., Talatahari S., Hamzehei-Javaran S. Generalized displacement control analysis and optimal design of geometrically nonlinear space structures. *Int J Comput Methods.* 2022. https://doi.org/10.1142/S0219876221430180.
44. Kaveh A., Talatahari S. Hybrid charged system search and particle swarm optimization for engineering design problems. *Eng Comput.* 2011; **28**(4):423–40. https://doi.org/10.1108/02644401111131876.
45. Kaveh A., Talatahari S. A charged system search with a fly to boundary method for discrete optimum design of truss structures. *Asian J Civ Eng (Building and Housing).* 2010; **11**(3):277–293.
46. Goodarzimehr V., Fazlı M., Fanaie N., Gandomi A. H. Enhanced special relativity search algorithm based on Lorentz force for structural optimization. *Int J Comput Methods.* 2024. https://doi.org/10.1142/S0219876224500646.